International Journal of Heat and Mass Transfer 115 (2017) 882–894

Contents lists available at ScienceDirect

International Journal of Heat and Mass Transfer

journal homepage: www.elsevier.com/locate/ijhmt

Element differential method for solving general heat conduction problems

Xiao-Wei Gao *, Shi-Zhang Huang, Miao Cui, Bo Ruan, Qiang-Hua Zhu, Kai Yang, Jun Lv, Hai-Feng Peng

Dalian University of Technology, State Key Laboratory of Structural Analysis for Industrial Equipment, School of Aeronautics and Astronautics, Dalian 116024, China

ARTICLE INFO

Article history:
Received 9 June 2017
Received in revised form 23 July 2017
Accepted 13 August 2017

Keywords:
Element differential method
EDM
Shape functions
Isoparametric elements
Heat conduction

ABSTRACT

In this paper, a new numerical method, Element Differential Method (EDM), is proposed for solving general heat conduction problems with variable conductivity and heat source subjected to various boundary conditions. The key aspect of this method is based on the direct differentiation of shape functions of isoparametric elements used to characterize the geometry and physical variables. A set of analytical expressions for computing the first and second order partial derivatives of the shape functions with respect to global coordinates are derived, which can be directly applied to governing differential equations and boundary conditions. A new collocation method is proposed to form the system of equations, in which the governing differential equation is collocated at nodes inside elements, and the flux equilibrium equation is collocated at interface nodes between elements and outer surface nodes of the problem. EDM is a strong-form numerical method. It doesn't require a variational principle or a control volume to set up the computational scheme, and no integration is involved. A number of numerical examples of two- and three-dimensional problems are given to demonstrate the correctness and efficiency of the proposed method.

1. Introduction

Heat conduction and other engineering problems are usually governed by a set of simultaneous second-order partial differential equations (PDEs), with a proper set of temperature (Dirichlet, essential) and flux (Neumann, natural) boundary conditions. Various numerical methods are available to solve these types of problems. The frequently used ones are the finite volume method (FVM) [1–4], finite difference method (FDM) [5–9], finite element method (FEM) [10–15], boundary element method (BEM) [16–22], and mesh free method (MFM) [23–28].

FVM and FDM are the frequently used methods in fluid mechanics as well as heat and mass transfer problems. FDM directly discretizes the governing differential equations based on the use of regularly distributed grids, while FVM works over the constructed control volume of each grid by employing the Gaussian integration principle to transform the flux-related terms in the governing equation to the boundary of the control volume. They have advantages of easily discretizing the governing equations and treating discontinuous physical phenomena, such as capturing shock waves and implementing upwind scheme. The main drawback of these two methods is that a lot of control volumes or points are required to achieve a satisfactory result, and the computational accuracy in heat flux on the boundary is poor [29–31].

FEM is the dominant method in the analysis of solid mechanics as well as other engineering problems. The distinct advantage of FEM is that almost any complicated engineering problems can be simulated using FEM. This feature is attributed to the use of various well-formed isoparametric elements which can be employed to discretize the geometry of the problem and interpolate physical variables. And, also because of using the isoparametric elements, the total numbers of elements and nodes required in FEM are much less than that used in FVM and FDM. The drawbacks of FEM are mainly embodied in the following aspects: (1) A variational or a virtual work principle is needed to establish the FEM formulation. Different problems have different representation forms of these principles, which gives rise to the inconvenience to set up a unified algorithm in handling multi-field coupling problems. (2) Domain integration for each of the elements is required, which sometimes is time consuming and different number of integration points (Gaussian points) may result in different computational accuracy of the variable gradients or stresses. (3) Too heavy distortion of the elements is prohibited to avoid the ill-condition of the element stiffness matrix.

* Corresponding author.
E-mail address: xwgao@dlut.edu.cn (X.-W. Gao).

http://dx.doi.org/10.1016/j.ijheatmasstransfer.2017.08.039
0017-9310/

It is worth mentioning that a new method, called the control volume finite element method (CVFEM), was proposed by Baliga and Patankar [32,33]. The CVFEM is a scheme that uses the advantages of both FVM for easy simulation of multi-physics problems and FEM for fitting complex geometries. This method has been well developed by Sheikholeslami and co-workers [34–37] for solving heat transfer and fluid dynamics.

Comparing to FEM, the BEM only needs to discretize the boundary of the problem into elements. This feature of BEM not only can reduce the dimensions of the problem by one, but also can easily simulate the heat and stress concentration behaviors [16,21]. The drawback of BEM is that a fundamental solution is required in setting up the BEM formulation, which is usually derived from a linear problem, and therefore it is difficult to establish a pure BEM algorithm for non-linear and non-homogeneous problems. Different from the above mentioned methods, MFM only needs a group of distributed points in the computational region, and therefore the distinct advantage of MFM is that problems with irregular geometries can be easily discretized. However, MFM has the drawbacks of time-consuming to form the global shape functions and difficulty to apply boundary conditions [23,24].

According to the formulation technique, the existing numerical methods can be roughly divided into two categories: weak-form and strong-form techniques [25]. In the weak-form technique, such as the FEM, BEM and part approaches of MFM, the governing PDE is solved indirectly, by converting it to a weak form using a mathematical principle, such as the variational principle, or an energy principle [10,12]. Attributing to the use of easily well-formed elements which can guarantee the variation of the physical variables to be consistent through element nodes, the weak-form technique usually results in very stable computational results.

In the strong-form technique, such as most approaches of MFM [25] and the conventional FDM, global shape functions are constructed by selecting a number of nodes around the node under consideration, and then, to form the final system of equations. The physical variables expressed in terms of the shape functions and their nodal values are directly substituted into the governing partial differential equations for each of the nodes in the interior of the domain, and into the relationships of boundary conditions about physical variables and their fluxes for all nodes on the boundary. Because all the equations (governing equations and boundary conditions) are all enforced at the nodes, this type of technique is usually called the collocation method [26,38]. The working process of this method is very straightforward, and can be easily coded for complicated multi-field problems. However, since there are no means to control the stability and the convergence of the solution, the collocation method is often found not stable and the solutions can vary a lot when the locations of the nodes change [25]. Besides, since the governing equations and the boundary conditions are entirely separately satisfied at individual nodes, there could be conflicts for nodes near the boundary. This disconnected situation could be one of the main causes of the instability issues in the collocation methods. Therefore, to ensure the stability of the solution, certain stabilization techniques must be used in the strong-form technique [23].

Recently, a different strong-form technique was proposed by Wen and Li [39–41], which is called the finite block method (FBM). A similar technique to FBM was proposed by Fantuzzi and Tornabene [42–44] for two-dimensional problems, which is called the strong formulation finite element method (SFEM). This type of methods incorporates the mapping technique proper of FEM and the strong form collocation approach. In these methods, isoparametric element-like blocks in FBM or sub-domains in SFEM are constructed based on the Lagrange interpolation formulation. In FBM, only the first order partial derivative of physical variables with respect to global coordinates is used and high order spatial derivatives are calculated through the recursive use of the first order derivative. In FBM and SFEM, the governing equation formulated using the constructed derivatives is applied to the internal nodes, and the specified boundary conditions on each block's/sub-domain's boundary are applied as independent equations. In this way, the formed final system of equations includes internal nodal temperatures and each block's boundary temperature and flux as unknowns. When solving a problem using FBM/SFEM, a few high order blocks, each having many nodes, are used to ensure the final system of equations not so large. As in other strong-form techniques, FBM/SFEM have the advantage of easy coding, but has the drawbacks of having too many unknowns in the system of equations and needing too many nodes over each block/sub-domain when solving a complicated practical engineering problem.

The motivation of this paper is to establish a numerical method which can be easily used as the collocation method and can result in stable computational results as FEM. To achieve this purpose, a new robust method, element differential method (EDM) [45], is proposed in this paper for solving general heat conduction problems based on the use of isoparametric elements as used in the standard FEM [4]. A set of explicit formulations of computing the first and second order spatial derivatives are derived for two-dimensional (2D) and three-dimensional (3D) problems. These formulations are expressed for shape functions of elements and therefore can be used to any physical variables' differentiation. EDM is a strong-form technique, which borrows the idea of FEM in the aspect of using isoparametric elements to obtain the spatial derivatives, and the idea of FBM/SFEM and collocation-like MFM in the aspect of collocating equations at nodes. The former (using elements) can result in very stable solutions and the latter (collocating at nodes) does not require any integration. Two distinct novelties can be found in the paper: (1) a set of analytical expressions of computing the second order spatial derivatives of shape functions for 3D problems are derived for the first time, which can make the computation more accurate and faster, and (2) a new collocation and assembling technique is proposed for forming the system of equations, which can make the system have the size as in the standard FEM, much smaller than in FBM and SFEM. Since EDM can use high order isoparametric elements to compute the spatial derivatives, the computational accuracy in heat flux is higher and the required total number of computational nodes are much less than the frequently used method (FVM) in heat transfer problems. The most important feature of the proposed method is that the derived spatial derivatives can be directly substituted into the governing equations and the heat flux equilibrium equations to form the final system of algebraic equations, and no any mathematical principles or integrations are required. Therefore, EDM is very easy to be coded in dealing with engineering problems with complicated governing equations and boundary conditions.

2. Governing equations for heat conduction problems

The governing equation for steady state heat conduction problems with a spatially varying thermal conductivity and heat source can be expressed as [27]

$$\nabla \cdot (\lambda \cdot \nabla T) + Q(x) = \frac{\partial}{\partial x_i}\left(\lambda_{ij}(x)\frac{\partial T(x)}{\partial x_j}\right) + Q(x) = 0 \tag{1}$$

The boundary conditions of the problem are

$$T(x) = \bar{T} \quad x \in \Gamma_1 \tag{2a}$$

$$q(x) = -\lambda_{ij}(x)\frac{\partial T(x)}{\partial x_j} n_i = \bar{q} \quad x \in \Gamma_2 \tag{2b}$$

$$q(x) = -\lambda_{ij}(x)\frac{\partial T(x)}{\partial x_j}n_i = h(T(x) - T_\infty) \quad x \in \Gamma_3 \tag{2c}$$

in which, $\Gamma_1 \cup \Gamma_2 \cup \Gamma_3 = \Gamma$, $\Gamma = \partial\Omega$, n is the outward normal to the boundary Γ, h is the heat transfer coefficient; $\bar{T}$, $\bar{q}$ and T_∞ are the prescribed temperature, heat flux and environmental temperature on the boundary, respectively; x_i is the i-th component of the spatial coordinates at point x, λ_{ij} the thermal conductivity, T the temperature, and Q the heat-generation rate. The repeated subscripts i and j represent the summation through its range which is 2 for 2D and 3 for 3D problems.

3. Derivatives of elemental shape functions with respect to global coordinates

The key task in solving PDEs is to accurately calculate the first and second order partial derivatives of unknown functions with respect to spatial coordinates, as appeared in Eqs. (1) and (2). The isoparametric elements used in FEM [10,11] have excellent characteristics in geometry representation and physical variable interpolation. The essential work of this paper is to derive a set of analytical expressions for computing the first and second partial derivatives needed in solving PDEs based on isoparametric elements.

3.1. Shape functions of isoparametric elements

To numerically compute the partial derivatives appearing in Eqs. (1) and (2), the isoparametric elements [10,11] are adopted herein. The key mathematical quantities characterizing the isoparametric elements are the shape function used to model the geometry and interpolate physical variables. The shape functions for 1D isoparametric elements can be determined by the Lagrange interpolation formulation:

$$L_I^m(\xi) = \prod_{i=1, i\neq I}^{m} \frac{\xi - \xi_i}{\xi_I - \xi_i} \quad (I = 1 \sim m, -1 \leqslant \xi \leqslant 1) \tag{3}$$

where m is the number of interpolation points, ξ is the isoparametric coordinate (which is also called the intrinsic or natural coordinate). For example, the shape functions for a 4-node line element (Fig. 1) can be expressed as follows:

$$\begin{aligned} L_1^4(\xi) &= \tfrac{1}{16}(1-\xi)[-10 + 9(\xi^2+1)] \\ L_2^4(\xi) &= \tfrac{9}{16}(1-\xi^2)(1-3\xi) \\ L_3^4(\xi) &= \tfrac{9}{16}(1-\xi^2)(1+3\xi) \\ L_4^4(\xi) &= \tfrac{1}{16}(1+\xi)[-10 + 9(\xi^2+1)] \end{aligned} \tag{4}$$

3.1.1. Shape functions for 2D and 3D isoparametric elements

The shape functions for 2D and 3D problems can be formed based on the 1D shape functions shown in Eq. (3). The rule of forming 2D and 3D shape functions can be found in [10,11], which can be expressed as follows:

$$N_\alpha(\xi, \eta) = L_I^m(\xi)L_J^n(\eta) \tag{5}$$

for 2D elements, and

$$N_\alpha(\xi, \eta, \zeta) = L_I^m(\xi)L_J^n(\eta)L_K^p(\zeta) \tag{6}$$

for 3D elements.

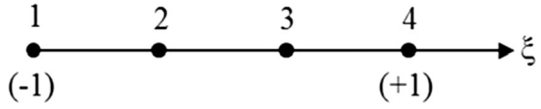

Fig. 1. 4-node 1D line element.

In Eqs. (5) and (6), the superscripts m, n, and p are the numbers of the interpolation points along ξ, η and ς directions, respectively, and the subscript α is determined by the permutation of the subscripts I, J, and K (for 3D case). Fig. 2 shows the 16-node 2D quadrilateral isoparametric element generated using Eq. (5) by setting m = 4 and n = 4, while Fig. 3 shows the 27-node 3D brick isoparametric element generated using Eq. (6) by setting m = 3, n = 3 and p = 3. As an example of the 16-node 2D element as shown in Fig. 2, the shape functions N_7 and N_{12} can be formed as $N_7(\xi, \eta) = L_3^4(\xi)L_2^4(\eta)$ and $N_{12}(\xi, \eta) = L_4^4(\xi)L_3^4(\eta)$.

3.1.2. Expressing coordinates and physical variables in terms of element nodal values

Any variables varying over an isoparametric element can be expressed in terms of their nodal values of the element [10]. For example, the spatial coordinates and temperature can be expressed as

$$x_i = N_\alpha x_i^\alpha, \quad T = N_\alpha T^\alpha \tag{7}$$

where x_i^α and T^α are the values of coordinates and temperature at node α, and the repeated index α represents the summation over all nodes.

3.2. Derivatives of shape functions with respect to global coordinates

To numerically compute the partial derivatives appearing in the governing equation (1) and boundary conditions (2), the analytical expressions for the first and second partial derivatives need to be derived. From Eq. (7) it follows that

$$\frac{\partial T}{\partial x_i} = \frac{\partial N_\alpha}{\partial x_i}T^\alpha, \quad \frac{\partial^2 T}{\partial x_i \partial x_j} = \frac{\partial^2 N_\alpha}{\partial x_i \partial x_j}T^\alpha \tag{8}$$

From Eqs. (3)–(6), it can be seen that N_α are the explicit functions of intrinsic coordinates ξ_k, thus

$$\frac{\partial N_\alpha}{\partial x_i} = \frac{\partial N_\alpha}{\partial \xi_k}\frac{\partial \xi_k}{\partial x_i} = [J]_{ik}^{-1}\frac{\partial N_\alpha}{\partial \xi_k} \tag{9}$$

$$\frac{\partial^2 N_\alpha}{\partial x_i \partial x_j} = \left[[J]_{ik}^{-1}\frac{\partial^2 N_\alpha}{\partial \xi_k \partial \xi_l} + \frac{\partial [J]_{ik}^{-1}}{\partial \xi_l}\frac{\partial N_\alpha}{\partial \xi_k}\right]\frac{\partial \xi_l}{\partial x_j} \tag{10}$$

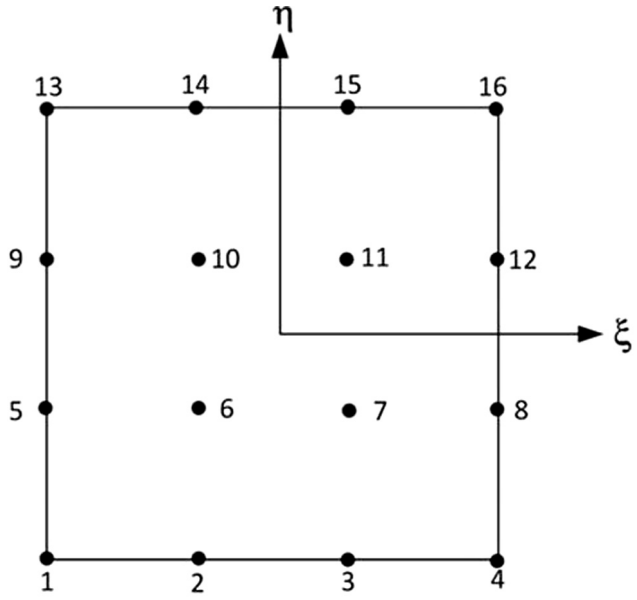

Fig. 2. 16-node 2D quadrilateral element.

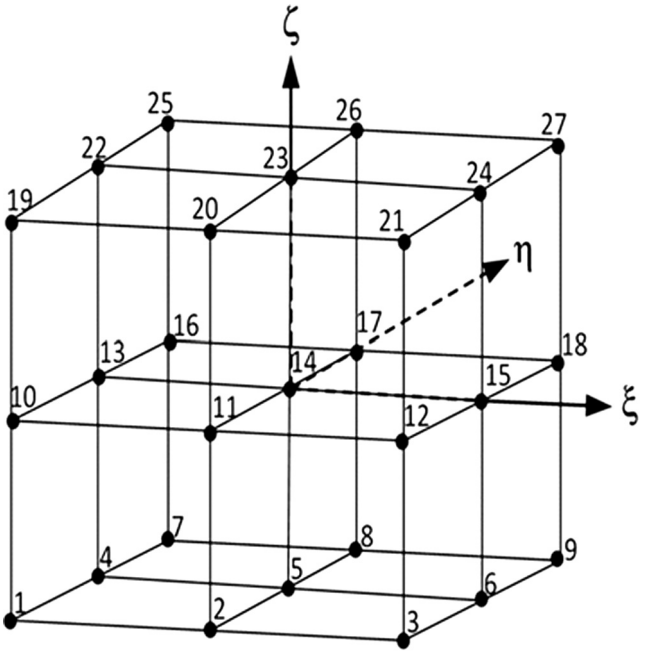

Fig. 3. 27-node 3D brick element.

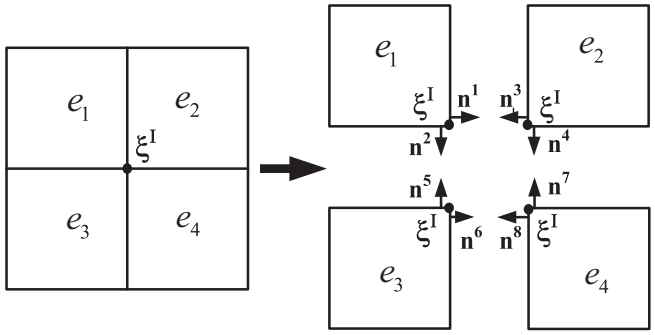

Fig. 4. Element surfaces associated with interface node ξ^I.

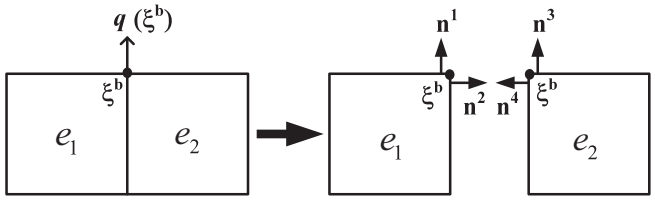

Fig. 5. Element surfaces associated with outer boundary node ξ^b.

where $[J]=[\partial x/\partial\xi]$ is the Jacobian matrix mapping from the global coordinate system x_i to the intrinsic coordinate system ξ_k, with $(x_1,x_2)=(x,y)$ and $(\xi_1,\xi_2)=(\xi,\eta)$ for 2D problems, and $(x_1,x_2,x_3)=(x,y,z)$ and $(\xi_1,\xi_2,\xi_3)=(\xi,\eta,\zeta)$ for 3D problems, and $\partial\xi_l/\partial x_j$ can be determined by the following matrix relationship [10,38,39]:

$$\left[\frac{\partial\xi}{\partial x}\right]=[J]^{-1}=\left[\frac{\partial x}{\partial\xi}\right]^{-1} \tag{11}$$

where

$$\left[\frac{\partial x}{\partial\xi}\right]_{ik}=\frac{\partial x_i}{\partial\xi_k}=\frac{\partial N_\alpha}{\partial\xi_k}x_i^\alpha \tag{12}$$

The terms $\frac{\partial N_\alpha}{\partial\xi_k}$ and $\frac{\partial^2 N_\alpha}{\partial\xi_k\partial\xi_l}$ in Eqs. (9) and (10) can be easily obtained by differentiating Eqs. (3)–(6), and the inverse and derivative matrixes of the Jacobian matrix [J] in the above equations can be derived as follows.

3.2.1. Inverse and derivatives of the Jacobian matrix [J] in 2D problems

For 2D problems, the inverse matrix $[J]^{-1}$ in Eqs. (9)–(11) can be easily derived [10,38,39] as

$$[J]^{-1}=\frac{1}{|J_2|}\begin{bmatrix}y_\eta & -y_\xi\\ -x_\eta & x_\xi\end{bmatrix},\quad |J_2|=x_\xi y_\eta-x_\eta y_\xi \tag{13}$$

in which, $x_\eta=\partial x/\partial\eta=(\partial N_\alpha/\partial\eta)x^\alpha$.

Also, the term $\partial[J]^{-1}_{ik}/\partial\xi_l$ in Eq. (10) can be derived from Eq. (13) as

$$\frac{\partial[J]^{-1}}{\partial\xi}=\frac{1}{|J_2|^2}\begin{bmatrix}(x_\eta y_{\xi\xi}+x_{\xi\eta}y_\xi-x_{\xi\xi}y_\eta)y_\eta-x_\eta y_\xi y_{\xi\eta}, & (x_{\xi\xi}y_\eta+x_\xi y_{\xi\eta}-x_\eta y_{\xi\xi})x_\eta-x_\xi x_{\xi\eta}y_\eta\\ (x_{\xi\xi}y_\eta+x_\xi y_{\xi\eta}-x_{\xi\eta}y_\xi)y_\xi-x_\xi y_\eta y_{\xi\xi}, & (x_{\xi\eta}y_\xi+x_\eta y_{\xi\xi}-x_\xi y_{\xi\eta})x_\xi-x_\eta x_{\xi\xi}y_\xi\end{bmatrix} \tag{14a}$$

$$\frac{\partial[J]^{-1}}{\partial\eta}=\frac{1}{|J_2|^2}\begin{bmatrix}(x_{\eta\eta}y_\xi+x_\eta y_{\xi\eta}-x_{\xi\eta}y_\eta)y_\eta-x_\eta y_\xi y_{\eta\eta}, & (x_{\xi\eta}y_\eta+x_\xi y_{\eta\eta}-x_\eta y_{\xi\eta})x_\eta-x_\xi y_\eta x_{\eta\eta}\\ (x_\xi y_{\eta\eta}+x_{\xi\eta}y_\eta-x_{\eta\eta}y_\xi)y_\xi-x_\xi y_\eta y_{\xi\eta}, & (x_{\eta\eta}y_\xi+x_\eta y_{\xi\eta}-x_\xi y_{\eta\eta})x_\xi-x_\eta x_{\xi\eta}y_\xi\end{bmatrix} \tag{14b}$$

3.2.2. Inverse and derivatives of the Jacobian matrix [J] in 3D problems

Similar to the 2D problems, the inverse matrix of the Jacobian matrix [J] for 3D problems can be derived as

$$[J]^{-1}=\frac{1}{|J_3|}[A] \tag{15}$$

where

$$[A]=\begin{bmatrix}y_\eta z_\zeta-y_\zeta z_\eta & y_\zeta z_\xi-y_\xi z_\zeta & y_\xi z_\eta-y_\eta z_\xi\\ x_\zeta z_\eta-x_\eta z_\zeta & x_\xi z_\zeta-x_\zeta z_\xi & x_\eta z_\xi-x_\xi z_\eta\\ x_\eta y_\zeta-x_\zeta y_\eta & x_\zeta y_\xi-x_\xi y_\zeta & x_\xi y_\eta-x_\eta y_\xi\end{bmatrix} \tag{16}$$

$$|J_3|=x_\xi y_\eta z_\zeta-x_\eta y_\xi z_\zeta-x_\xi y_\zeta z_\eta+x_\zeta y_\xi z_\eta+x_\eta y_\zeta z_\xi-x_\zeta y_\eta z_\xi \tag{17}$$

Differentiating Eq. (15) with respect to ξ_k, it follows that

$$\frac{\partial[J]^{-1}}{\partial\xi_k}=\frac{1}{|J_3|}\frac{\partial[A]}{\partial\xi_k}-\frac{1}{|J_3|^2}\frac{\partial|J_3|}{\partial\xi_k}[A] \tag{18}$$

From Eqs. (16) and (17), the following expressions can be derived

$$\frac{\partial[A]}{\partial\xi}=\begin{bmatrix}y_{\eta\xi}z_\zeta+y_\eta z_{\zeta\xi}-y_{\zeta\xi}z_\eta-y_\zeta z_{\eta\xi} & y_{\zeta\xi}z_\eta+y_\zeta z_{\xi\eta}-y_{\xi\xi}z_\zeta-y_\xi z_{\zeta\xi} & y_{\xi\xi}z_\eta+y_\xi z_{\eta\xi}-y_{\eta\xi}z_\xi-y_\eta z_{\xi\xi}\\ x_{\zeta\xi}z_\eta+x_\zeta z_{\eta\xi}-x_{\eta\xi}z_\zeta-x_\eta z_{\zeta\xi} & x_{\xi\xi}z_\zeta+x_\xi z_{\zeta\xi}-x_{\zeta\xi}z_\xi-x_\zeta z_{\xi\xi} & x_{\eta\xi}z_\xi+x_\eta z_{\xi\xi}-x_{\xi\xi}z_\eta-x_\xi z_{\eta\xi}\\ x_{\eta\xi}y_\zeta+x_\eta y_{\zeta\xi}-x_{\zeta\xi}y_\eta-x_\zeta y_{\eta\xi} & x_{\zeta\xi}y_\xi+x_\zeta y_{\xi\xi}-x_{\xi\xi}y_\zeta-x_\xi y_{\zeta\xi} & x_{\xi\xi}y_\eta+x_\xi y_{\eta\xi}-x_{\eta\xi}y_\xi-x_\eta y_{\xi\xi}\end{bmatrix} \tag{19a}$$

$$\frac{\partial[A]}{\partial\eta}=\begin{bmatrix}y_{\eta\eta}z_\zeta+y_\eta z_{\zeta\eta}-y_{\zeta\eta}z_\eta-y_\zeta z_{\eta\eta} & y_{\zeta\eta}z_\xi+y_\zeta z_{\xi\eta}-y_{\xi\eta}z_\zeta-y_\xi z_{\zeta\eta} & y_{\xi\eta}z_\eta+y_\xi z_{\eta\eta}-y_{\eta\eta}z_\xi-y_\eta z_{\xi\eta}\\ x_{\eta\zeta}z_\eta+x_\zeta z_{\eta\eta}-x_{\eta\eta}z_\zeta-x_\eta z_{\eta\zeta} & x_{\xi\eta}z_\zeta+x_\xi z_{\zeta\eta}-x_{\zeta\eta}z_\xi-x_\zeta z_{\xi\eta} & x_{\eta\eta}z_\xi+x_\eta z_{\xi\eta}-x_{\xi\eta}z_\eta-x_\xi z_{\eta\eta}\\ x_{\eta\eta}y_\zeta+x_\eta y_{\zeta\eta}-x_{\zeta\eta}y_\eta-x_\zeta y_{\eta\eta} & x_{\zeta\eta}y_\xi+x_\zeta y_{\xi\eta}-x_{\xi\eta}y_\zeta-x_\xi y_{\zeta\eta} & x_{\xi\eta}y_\eta+x_\xi y_{\eta\eta}-x_{\eta\eta}y_\xi-x_\eta y_{\xi\eta}\end{bmatrix} \tag{19b}$$

$$\frac{\partial[A]}{\partial\zeta}=\begin{bmatrix}y_{\eta\zeta}z_\zeta+y_\eta z_{\zeta\zeta}-y_{\zeta\zeta}z_\eta-y_\zeta z_{\eta\zeta} & y_{\zeta\zeta}z_\xi+y_\zeta z_{\xi\zeta}-y_{\xi\zeta}z_\zeta-y_\xi z_{\zeta\zeta} & y_{\xi\zeta}z_\eta+y_\xi z_{\eta\zeta}-y_{\eta\zeta}z_\xi-y_\eta z_{\xi\zeta}\\ x_{\zeta\zeta}z_\eta+x_\zeta z_{\eta\zeta}-x_{\eta\zeta}z_\zeta-x_\eta z_{\zeta\zeta} & x_{\xi\zeta}z_\zeta+x_\zeta z_{\xi\zeta}-x_{\zeta\zeta}z_\xi-x_\zeta z_{\xi\zeta} & x_{\eta\zeta}z_\xi+x_\eta z_{\xi\zeta}-x_{\xi\zeta}z_\eta-x_\xi z_{\eta\zeta}\\ x_{\eta\zeta}y_\zeta+x_\eta y_{\zeta\zeta}-x_{\zeta\zeta}y_\eta-x_\zeta y_{\eta\zeta} & x_{\zeta\zeta}y_\xi+x_\zeta y_{\xi\zeta}-x_{\xi\zeta}y_\zeta-x_\xi y_{\zeta\zeta} & x_{\xi\zeta}y_\eta+x_\xi y_{\eta\zeta}-x_{\eta\zeta}y_\xi-x_\eta y_{\xi\zeta}\end{bmatrix} \tag{19c}$$

and

$$\begin{aligned}\frac{\partial|J_3|}{\partial\xi}=&x_{\xi\xi}y_\eta z_\zeta+x_\xi y_{\eta\xi}z_\zeta+x_\xi y_\eta z_{\xi\zeta}-x_{\eta\xi}y_\xi z_\zeta-x_\eta y_{\xi\xi}z_\zeta-x_\eta y_\xi z_{\zeta\xi}\\&-x_{\xi\xi}y_\zeta z_\eta-x_\xi y_{\zeta\xi}z_\eta-x_\xi y_\zeta z_{\eta\xi}+x_{\zeta\xi}y_\xi z_\eta+x_\zeta y_{\xi\xi}z_\eta+x_\zeta y_\xi z_{\eta\xi}\\&+x_{\eta\xi}y_\zeta z_\xi+x_\eta y_{\zeta\xi}z_\xi+x_\eta y_\zeta z_{\xi\xi}-x_{\zeta\xi}y_\eta z_\xi-x_\zeta y_{\eta\xi}z_\xi-x_\zeta y_\eta z_{\xi\xi}\end{aligned} \tag{20a}$$

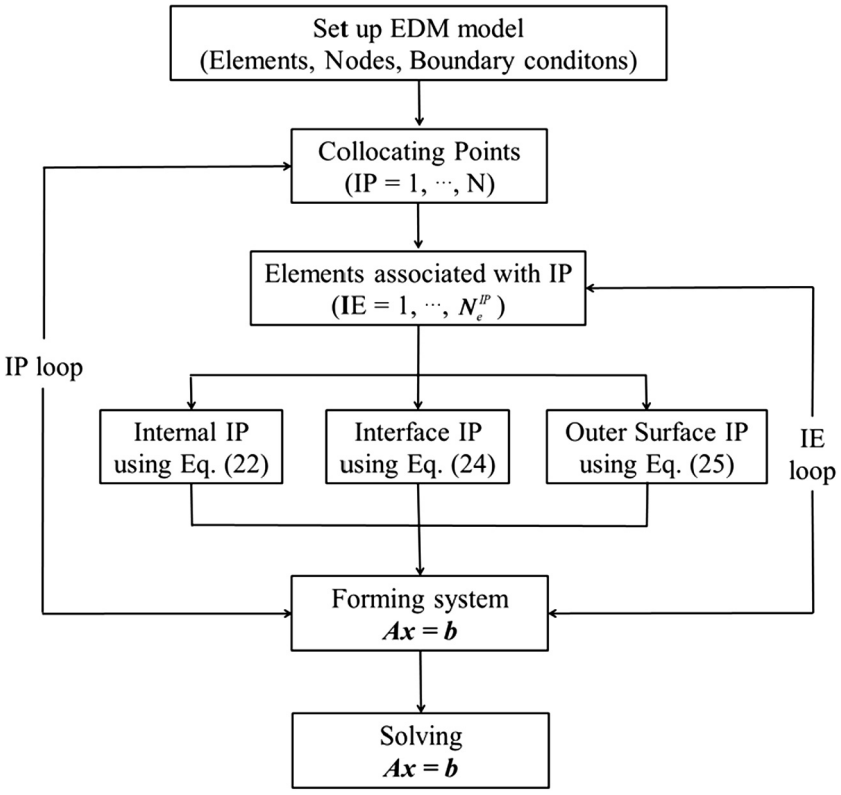

Fig. 6. Flowchart of the proposed scheme.

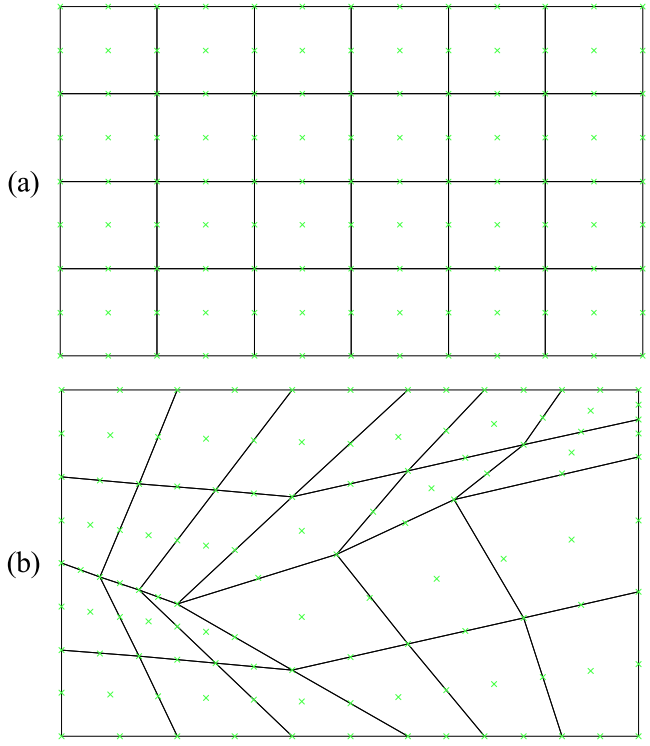

Fig. 7. EDM models of 9-node quadrilateral elements: (a) regular mesh; (b) distorted mesh.

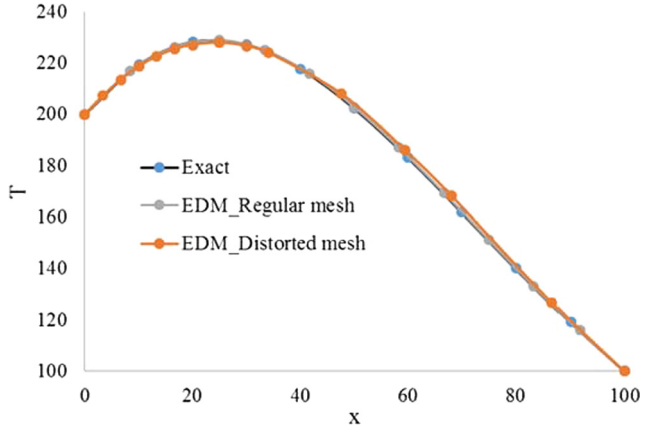

Fig. 8. Computed temperature along the middle line of the plate.

$$\frac{\partial |J_3|}{\partial \eta} = x_{\xi\eta}y_\eta z_\zeta + x_\xi y_{\eta\eta} z_\zeta + x_\xi y_\eta z_{\zeta\eta} - x_{\eta\eta}y_\xi z_\zeta - x_\eta y_{\xi\eta} z_\zeta - x_\eta y_\xi z_{\zeta\eta} - x_{\xi\eta}y_\zeta z_\eta - x_\xi y_{\zeta\eta} z_\eta - x_\xi y_\zeta z_{\eta\eta} + x_{\zeta\eta}y_\xi z_\eta + x_\zeta y_{\xi\eta} z_\eta + x_\zeta y_\xi z_{\eta\eta} + x_{\eta\eta}y_\zeta z_\xi + x_\eta y_{\zeta\eta} z_\xi + x_\eta y_\zeta z_{\xi\eta} - x_{\zeta\eta}y_\eta z_\xi - x_\zeta y_{\eta\eta} z_\xi - x_\zeta y_\eta z_{\xi\eta} \tag{20b}$$

$$\frac{\partial |J_3|}{\partial \zeta} = x_{\xi\zeta}y_\eta z_\zeta + x_\xi y_{\eta\zeta} z_\zeta + x_\xi y_\eta z_{\zeta\zeta} - x_{\eta\zeta}y_\xi z_\zeta - x_\eta y_{\xi\zeta} z_\zeta - x_\eta y_\xi z_{\zeta\zeta} - x_{\xi\zeta}y_\zeta z_\eta - x_\xi y_{\zeta\zeta} z_\eta - x_\xi y_\zeta z_{\eta\zeta} + x_{\zeta\zeta}y_\xi z_\eta + x_\zeta y_{\xi\zeta} z_\eta + x_\zeta y_\xi z_{\eta\zeta} + x_{\eta\zeta}y_\zeta z_\xi + x_\eta y_{\zeta\zeta} z_\xi + x_\eta y_\zeta z_{\xi\zeta} - x_{\zeta\zeta}y_\eta z_\xi - x_\zeta y_{\eta\zeta} z_\xi - x_\zeta y_\eta z_{\xi\zeta} \tag{20c}$$

Using above analytical expressions, the first and second order spatial derivatives of shape functions can be calculated and a system of equations can be formed by substituting these spatial derivatives into the governing equation and boundary conditions.

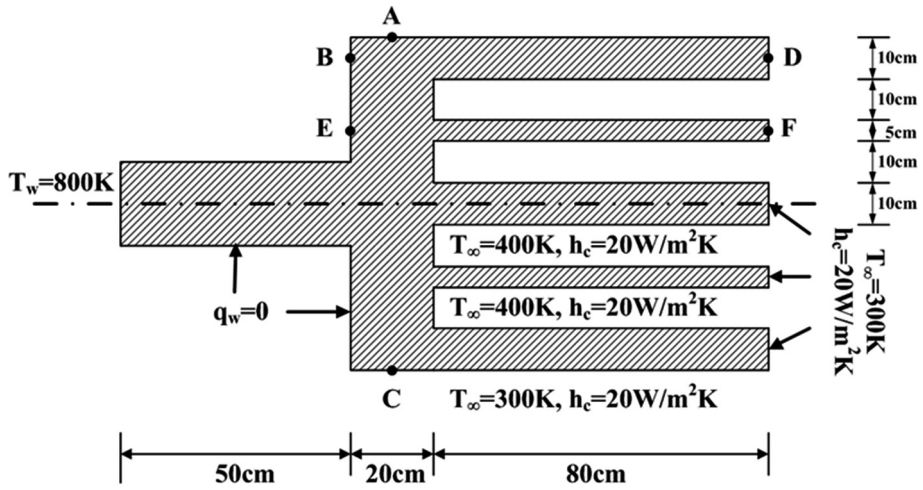

Fig. 9. Geometry and boundary conditions for the heat radiating fin.

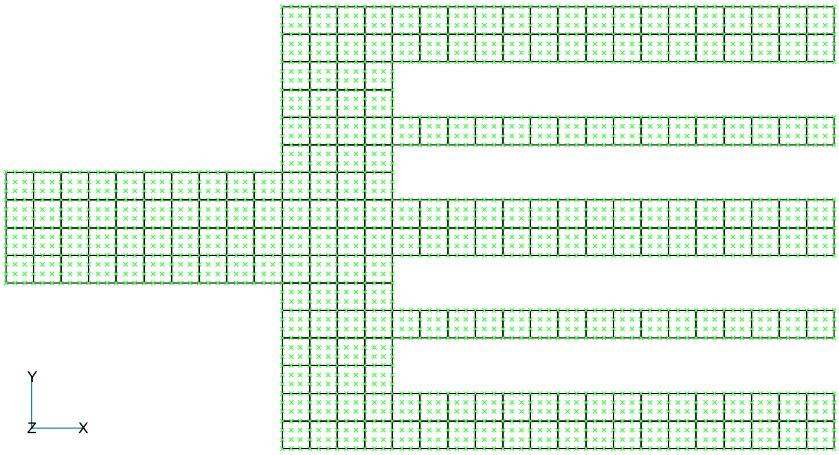

Fig. 10. EDM mesh of 16-node quadrilateral elements.

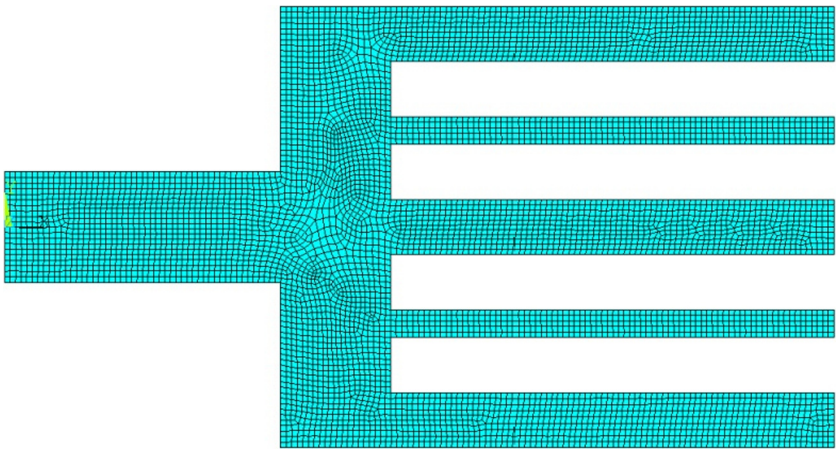

Fig. 11. FEM mesh of 8-node quadrilateral elements.

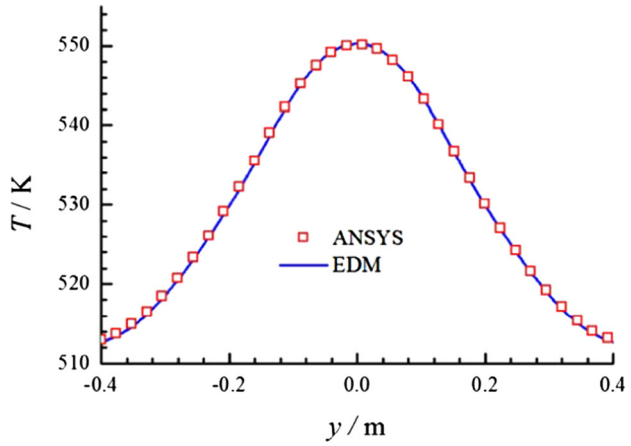

(a) Temperature along line AC

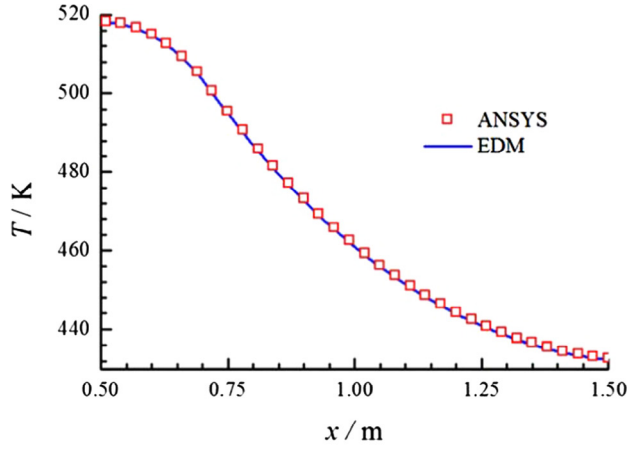

(b) Temperature along line BD

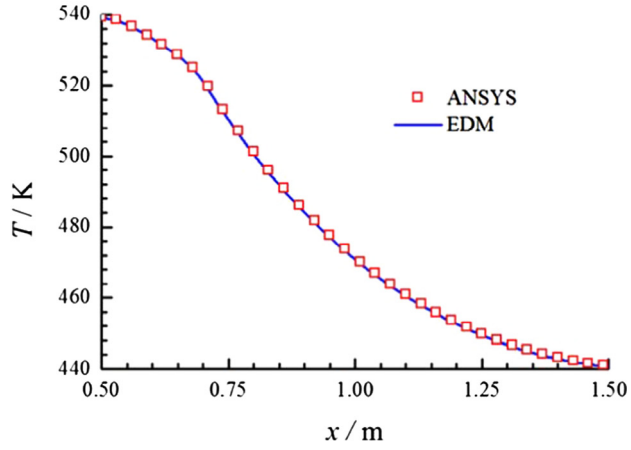

(c) Temperature along line EF

Fig. 12. Temperature distribution along lines marked in Fig. 9.

4. Assembling system of equations from governing equations and boundary conditions

When solving a boundary value problem governed by a partial differential equation using EDM, the computational domain needs to be discretized into a series of isoparametric elements and nodes as done in FEM. The first and second spatial derivatives of physical variables can be calculated using Eqs. (7)–(10). Based on this, a system of equations can be directly formed by substituting Eq. (8) into the governing equation for internal nodes and boundary conditions for boundary nodes.

4.1. Setting up equations for internal nodes of elements based on the governing differential equation

For nodes located within an element, the governing equation (1) should be satisfied. To facilitate the use of EDM, Eq. (1) can be written as

$$\frac{\partial \lambda_{ij}(x)}{\partial x_i}\frac{\partial T(x)}{\partial x_j} + \lambda_{ij}(x)\frac{\partial^2 T(x)}{\partial x_i \partial x_j} + Q(x) = 0 \tag{21}$$

Substituting Eq. (8) into Eq. (21) leads to

$$\left[\frac{\partial \lambda_{ij}(\xi)}{\partial x_i}\frac{\partial N_\alpha(\xi)}{\partial x_j} + \lambda_{ij}(\xi)\frac{\partial^2 N_\alpha(\xi)}{\partial x_i \partial x_j}\right]T^\alpha + Q(\xi) = 0 \quad \xi \in \Omega \tag{22}$$

where ξ is the intrinsic coordinate at the node inside the element under considered, with $\xi = (\xi, \eta)$ for 2D, and $\xi = (\xi, \eta, \varsigma)$ for 3D problems. For each internal node, we can set up an equation using Eq. (22), which is formulated in terms of the element nodal values of temperature.

The term $\partial \lambda_{ij}/\partial x_i$ in Eq. (22) can be calculated through direct differentiation, if the analytical expression of the heat conductivity λ_{ij} is given, otherwise the following expression can be used to compute its value.

$$\frac{\partial \lambda_{ij}(\xi)}{\partial x_i} = \frac{\partial N_\beta(\xi)}{\partial x_i}\lambda_{ij}^\beta \tag{23}$$

where λ_{ij}^β is the value of λ_{ij} at the element node β.

4.2. Setting up equations for element interface nodes based on flux equilibrium conditions

For a node located on the interface shared by a few elements, the relationship between the flux and temperature gradient, i.e. Eq. (2b), is applied to each surface including the node. In terms of the flux equilibrium condition $\sum_{f=1}^{M} q^f(\xi^I) = 0$, the following equation can be set up by substituting Eq. (8) into Eq. (2):

$$\sum_{f=1}^{M} -\lambda_{ij}(\xi^I)\frac{\partial N_\alpha(\xi^I)}{\partial x_j} n_i^f(\xi^I) T^\alpha = 0 \quad \xi^I \in \Gamma_I \tag{24}$$

where M is the number of element surfaces associated with the interface node denoted by the intrinsic coordinate ξ^I which is different for different elements, the n_i^f is the outward normal to the surface f. and Γ_I represents the interface between elements. Fig. 4 shows a 2D case for the interface node ξ^I shared by 4 elements, e_1 - e_4, with 8 surfaces (M = 8) symbolled using n^1–n^8.

4.3. Setting up equations for outer boundary nodes based on flux equilibrium conditions

For a node located on the outer boundary of the problem, the heat flux equilibrium condition $\sum_{f=1}^{K} q^f(\xi^b) = q(\xi^b)$ is used, where K is the number of element surfaces associated with the boundary node ξ^b, and q is the external heat flux. Thus, substituting Eq. (8) into Eq. (2), it follows that

$$\sum_{f=1}^{K} -\lambda_{ij}(\xi^b)\frac{\partial N_\alpha(\xi^b)}{\partial x_j} n_i^f(\xi^b) T^\alpha = q(\xi^b) \tag{25}$$

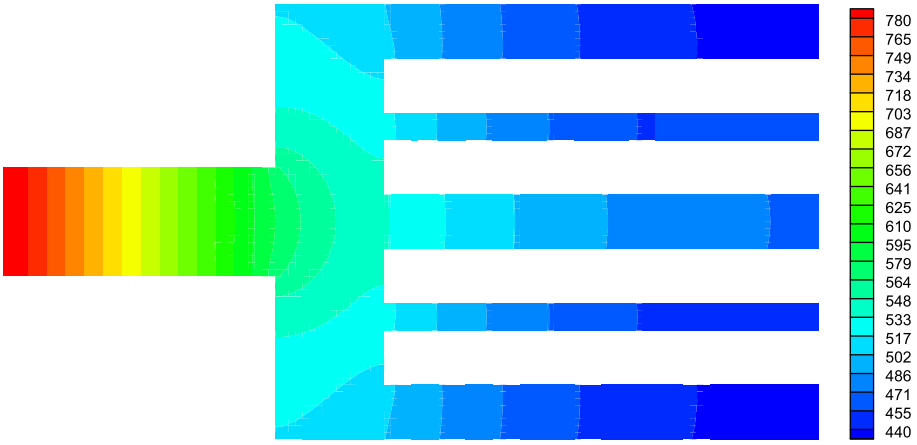

Fig. 13. Contour plot of the temperature over the heat radiating fin.

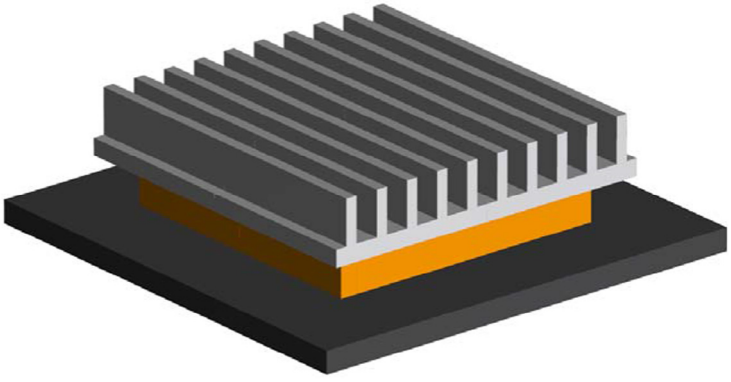

(a) 3D view of the CPU radiator

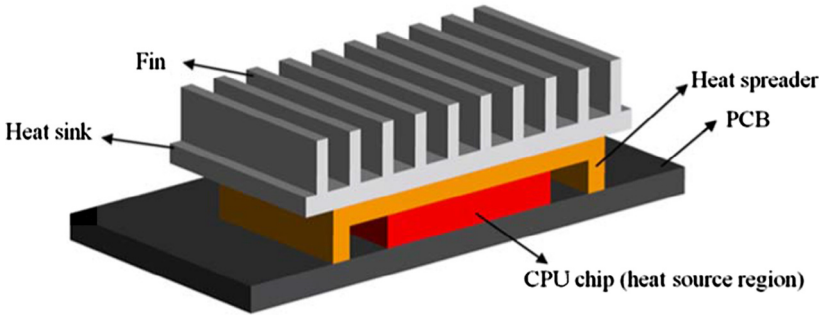

(b) Sectional view and components

Fig. 14. The CPU radiator: (a) 3D view; (b) Sectional view and components.

Table 1
Geometry and material parameters of related components.

Component	Size (mm)	Thermal conductivity (W/mK)
Fin	$30 \times 1 \times 4$	240
Heat sink	$30 \times 30 \times 1.5$	240
Heat spreader	$25 \times 25 \times 1.5$; $25 \times 2 \times 1.5$	390
CPU chip	$15 \times 15 \times 2.5$	82
PCB	$40 \times 40 \times 2$	8.37

Table 2
Numbers of elements and nodes for three sets of 27-node computational meshes.

Mesh	No. of elements	No. of nodes
Mesh-1	6048	61,580
Mesh-2	15,205	139,736
Mesh-3	121,640	1,045,024

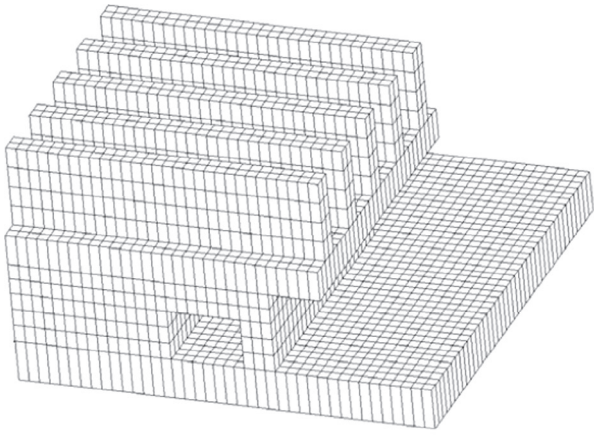

(a) Mesh-1

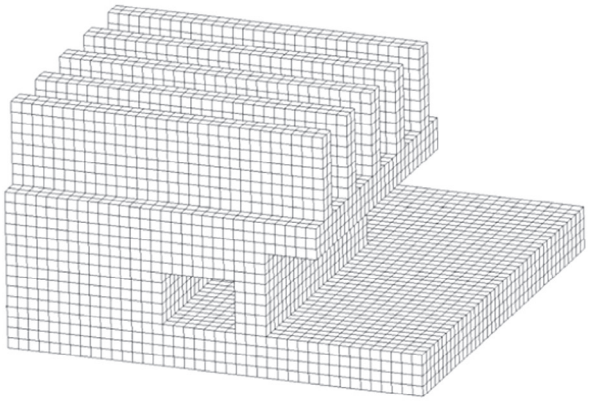

(b) Mesh-2

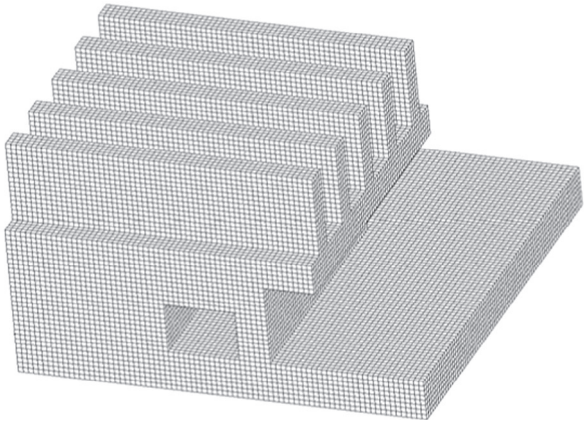

(c) Mesh-3

Fig. 15. Computational meshes used in EDM.

where $q(\xi^b) = \bar{q}$, for $\xi^b \in \Gamma_2$; and $q(\xi^b) = h((\xi^b) - T_\infty)$, for $\xi^b \in \Gamma_3$. Fig. 5 shows a 2D case for the boundary node ξ^b shared by 2 elements, e_1 - e_2, with 4 surfaces ($K = 4$).

4.4. Forming the final system of equations

Applying ξ in Eq. (22) to all internal nodes and ξ^I in Eq. (24) to all interface nodes of all elements, each of these nodes can generate an equation involving nodal values of temperature over all nodes of the elements including the considered node. And apply ξ^b in Eq. (25) to all outer boundary nodes, each of them can generate an equation involving nodal temperatures and heat fluxes. We can define a global nodal vector of temperature, numbered in the global node sequence. Each of the element nodes α in Eqs. (22)–(25) corresponds to one position of the global nodes. For interface nodes shared by a few elements, the temperature continuous condition, $T^I = T^{II}$, is used, where T^I and T^{II} are the temperatures over the adjacent elements I and II, respectively, and they occupy the same position in the global temperature vector. The unknowns in the final system of equations are numbered in the global node sequence. For each outer boundary node, either the temperature or the heat flux is specified. Thus, multiplying the specified temperatures and fluxes in Eqs. (22)–(25) with corresponding coefficients to form a known vector b and moving it to the right-hand side of the system of equations, and the remaining terms in Eqs. (22)–(25) associated with unknown temperatures and unknown fluxes being put on the left-hand side of the system of equations, the final system of equations can be formed as

$$\boldsymbol{A}\boldsymbol{x} = \boldsymbol{b} \tag{26}$$

where $\boldsymbol{x}$ is a vector containing each nodal unknown temperature or unknown flux. By solving Eq. (26) for vector $\boldsymbol{x}$, we can obtain all unknowns of the problem. It is noted that if the total number of all nodes used to discretize the problem is N, then the size of the coefficient matrix $\boldsymbol{A}$ in Eq. (26) is $N \times N$. Since each equation in Eq. (25) is only related to the nodes of elements associated with the node collocated to this equation, the matrix $\boldsymbol{A}$ is sparse. This feature is in favor of applying a robust sparse matrix equation solver to solve Eq. (26). Fig. 6 is a flowchart of the above described scheme, in which $\boldsymbol{N}_e^{IP}$ is the number of all elements associated with the collocation point IP.

5. Numerical examples

To verify the correctness and demonstrate the potential of the proposed method, three numerical examples are given.

5.1. Example 1: Heat conduction over a rectangular plate

The first example considered is a plate of 100 cm × 60 cm with varying conductivity and heat source along the x-direction (horizontal direction) as follows:

$$\lambda_{ij}(\boldsymbol{x}) = \left(1 + \frac{x}{100}\right)^3 \delta_{ij} \quad Q(\boldsymbol{x}) = \frac{x}{100}\left(1 - \frac{x}{100}\right)$$

The top and bottom sides are insulated, while the left and right walls are imposed with the temperature conditions of 200 °C and 100 °C, respectively. The plate is discretized into 24 9-node 2D rectangular elements with 117 nodes (Fig. 7). A regular mesh and a distorted mesh are used in the computation to examine the stability of the computational results. Fig. 8 shows the computed temperature along the middle line of the plate using these two meshes. For this problem, the exact solution can be integrated [27] as follows.

$$T(\boldsymbol{x}) = \frac{100}{3}\left\{x - \frac{5000(950 + 3C_1 + 12x}{(100 + x)^2} - 450Log(100 + x)\right\} + C_2$$

where

$$C_1 = 400Log(2) - \tfrac{2474}{9}$$
$$C_2 = \tfrac{200}{9}\{103 + 2250Log(2) + 1350Log(5)\}$$

For the comparison purpose, the exact solution is also plotted in Fig. 8. From Fig. 8, it can be seen that the computed results are in

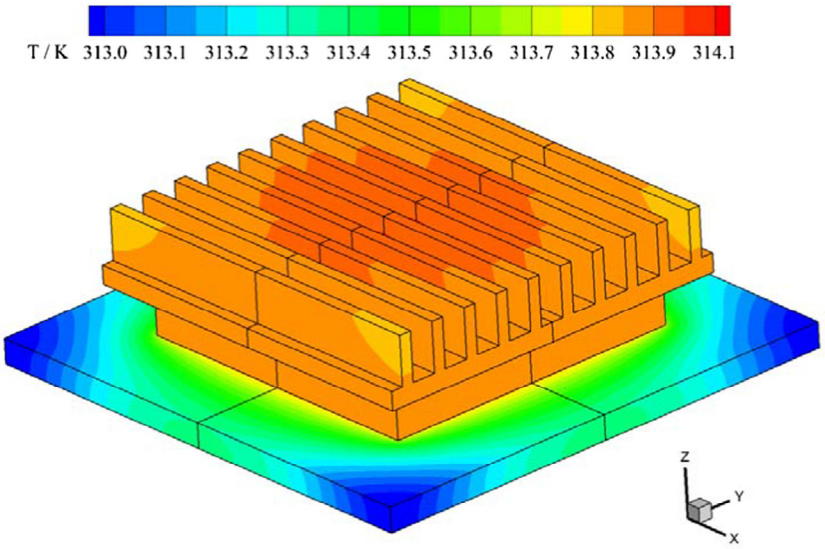

(a) Overall view of the temperature distribution

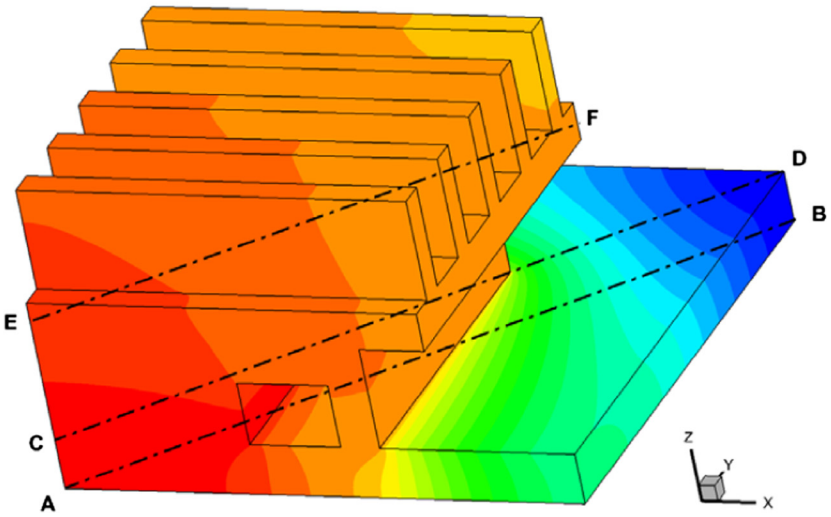

(b) Temperature over a quarter of the radiator

Fig. 16. Contour plot of the computed temperature: (a) overall view; (b) a quarter.

good agreement with the exact ones even for the highly distorted mesh. This indicates that the proposed method is correct and the computational results are stable for different meshes. On the other hand, from Fig. 8 it can be seen that the maximum temperature occurs within the plate, rather than on the right-hand side where the maximum temperature boundary condition is imposed. This phenomenon is due to the heat source which has larger value inside the plate than on the boundary.

5.2. Example 2: Heat conduction over a radiating fin

The second example concerned with is a heat radiating fin exposed in an environment. The geometry and boundary conditions are shown in Fig. 9. The left side of the fin is specified with temperature of 800 K and the other surfaces of the left part are heat insulated. The top, bottom and right sides of the right part of the fin are subjected to the convective boundary conditions of h = 20 W/m2 K, $T_\infty = 300$ K, while the inner surfaces are h = 20 W/m2 K, $T_\infty = 400$ K. The heat conductivity of the fin is λ = 200 W/mK. To perform the analysis using EDM, the fin is discretized into 232 16-node quadrilateral elements with 2419 nodes as shown in Fig. 10. For comparison, the problem is also computed using the FEM software ANSYS. Fig. 11 shows the ANSYS mesh of 5930 nodes.

Fig. 12 gives the computed temperature distributed along the lines marked in Fig. 9, and Fig. 13 is the contour plot of the computed temperature using EDM. From Fig. 12, it can be seen that the computed temperature using the current method EDM are in excellent agreement with that using the commercial software ANSYS. On the other hand, from Fig. 12(a) it can be seen that the temperature distribution is symmetric about the middle line. This is because the geometry and the boundary condition are symmetric about the middle line. And, Fig. 13 shows that the temperature over the plate decrease from the left side to the right side. This phenomenon coincides with the imposed boundary condition and qualitatively validates the correctness of the proposed method.

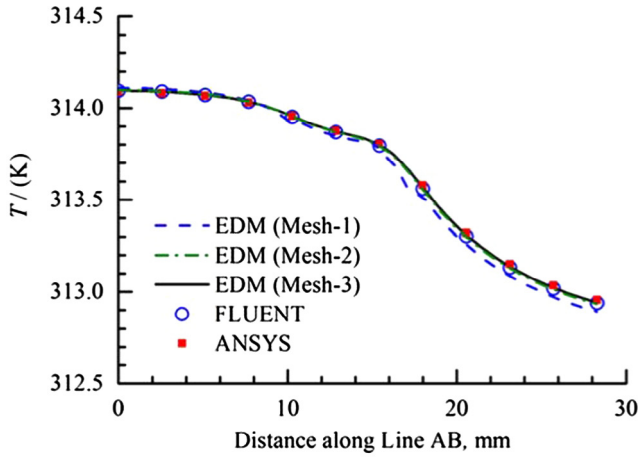

(a) Temperature along Line AB

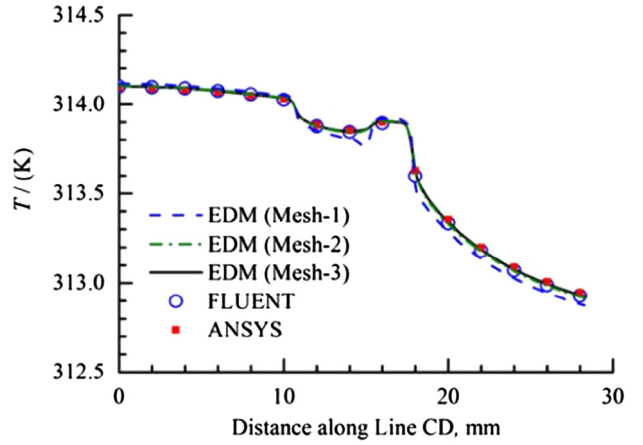

(b) Temperature along Line CD

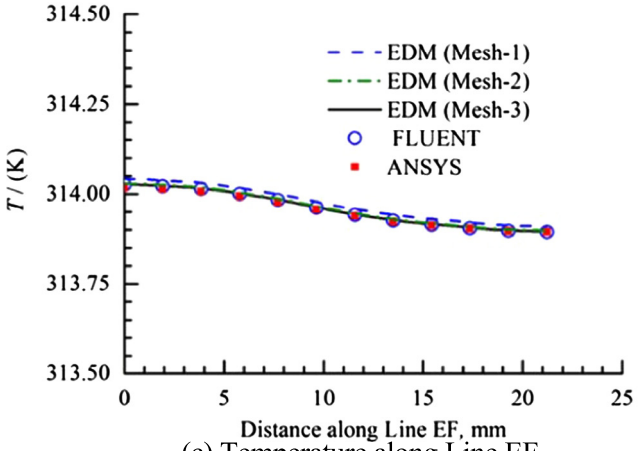

(c) Temperature along Line EF

Fig. 17. Temperature distribution along lines marked in Fig. 16(b): (a) along Line AB; (b) along Line CD; (c) along Line EF.

5.3. Example 3: Heat conduction over a heat radiator

The third example is on the heat conduction through a heat radiator of CPU, which is aimed to show the application potential of EDM to solve practical engineering problems. The geometry and detailed components of the radiator are shown in Fig. 14, and the related geometry and material parameters of all components are displayed in Table 1. A uniform heat source of

Table 3
Computed temperature at three selected points using different methods (unit: K).

Method	Point A	Point D	Point F
EDM (Mesh-1)	314.115	312.875	313.911
EDM (Mesh-2)	314.096	312.916	313.898
EDM (Mesh-3)	314.094	312.925	313.895
ANSYS	314.086	312.937	313.893
FLUENT	314.092	312.923	313.894

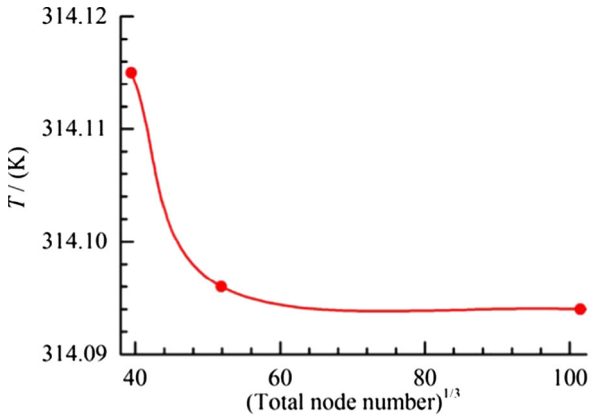

(a) Point A

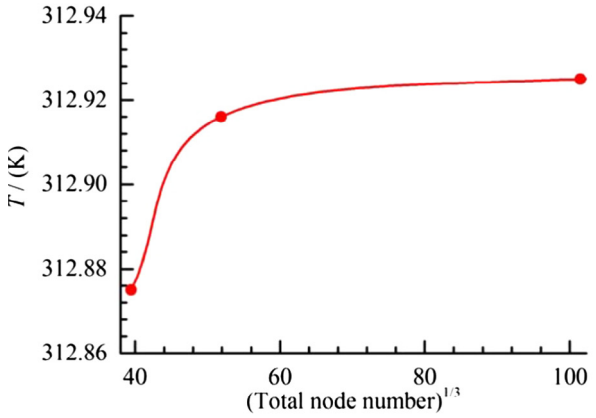

(b) Point D

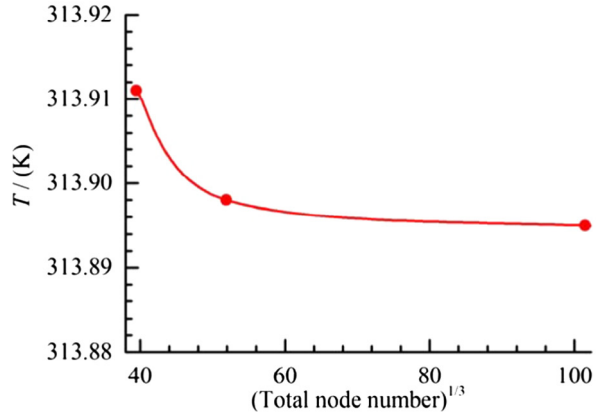

(c) Point F

Fig. 18. Convergence of results with respect to cube root of the number of nodes.

1.788E6 W/m3 generated by CPU is applied in the region of the CPU chip. All surfaces exposed in the air are specified as the convective heat transfer boundary condition with an environment temperature of $T_\infty = 298.15$ K and the heat transfer coefficient of h = 10 W/m2 K. The bottom of the printed circuit board (PCB) is insulated. Due to symmetry, only a quarter of the radiator is analyzed. In order to investigate the mesh independence of the computational results, three sets of 27-node computational meshes with different numbers of elements and nodes are employed as displayed in Table 2 and Fig. 15.

For comparison, the problem is also computed using the standard FEM software ANSYS and FVM software FLUENT. Fig. 16 is the contour plot of the computed temperature using EDM based on Mesh-3. Fig. 17 shows the distribution of the computed temperature from different methods along three lines AB, CD and EF as marked in Fig. 16(b). Table 3 gives the computed results at three selected points A, D and F, while Fig. 18 is a convergence curve of the results with respect to cube root of the number of nodes.

From Table 3 and Fig. 18, it can be seen that the convergence of the computational results is excellent. The results computed with Mesh-2 and Mesh-3 are almost no difference. On the other hand, from Fig. 17 it can be seen that the computed temperature using the current method EDM are in excellent agreement with those using the FEM-based software ANSYS and the FVM-based software FLUENT. The maximum relative error of the EDM results with mesh-2 and mesh-3 is within 0.007% compared to the results of ANSYS and FLUENT. This indicates that the present method is correct and can be used to solve complicated engineering problems.

From Fig. 16 it can be seen that the high temperature area is around the center part of the heat radiator where the CPU chip is located. However, Table 3 shows that the temperature does not change so large over the whole heat radiator, although the heat source (CPU chip) exists. This indicate that the material of the radiator has an excellent heat radiating property.

6. Concluding discussions

A new method, element differential method, has been proposed for solving general second order PDEs based on the use of isoparametric elements, and a robust assembling technique is developed for establishing the algebraic system of equations. The following conclusions and discussions can be drawn:

(1) The method belongs to the categories of FEM, FBM, and the collocation method, but it is easier to be coded than FEM, and is able to generate smaller system and more accurate results than FBM, and can obtain more stable solutions than the collocation method.
(2) Since EDM adopts the isoparametric elements to discretize the geometry of the problem and express physical variables, the specified boundary conditions can be directly imposed.
(3) The analytical expressions of computing spatial derivatives are only derived for the first and second order derivatives. If high order differential equations will be solved using EDM, the related high order derivatives can be generated by recursively using the first and second derivative expressions as done in FBM.
(4) Since the governing equation is only applied to the nodes inside elements, if the problem solved has heat sources, the elements having internal nodes should be used. The elements constructed using the Lagrange interpolation formulation, as done in the paper, can satisfy this requirement.
(5) The system of equations established in this paper is formulated in terms of temperature and heat flux vectors. It is similar to that generated in BEM [46], so EDM can be directly combined with BEM to solve complicated problems.
(6) The method presented in the paper is only for spatial discretization. For time-dependent problems, the time derivatives also need to be handled; and for nonlinear problems, in iterative process is also needed for solving the system of equations. The techniques to handle these two types of problems are essentially the same as those used in the standard FEM and FVM, which are already well developed and can be naturally extended to the methods proposed in this paper.

Acknowledgment

The support of this investigation by the National Natural Science Foundation of China under Grant Nos. 11672061, 51576026, 11502047 is gratefully acknowledged.

Conflict of interest

The authors declare that they have no conflict of interests.

References

[1] W.Q. Tao, Y.L. He, Q.W. Wang, Z.G. Qu, F.Q. Song, A unified analysis on enhancing single phase convective heat transfer with field synergy principle, Int. J. Heat Mass Transf. 45 (2002) 4871–4879.
[2] J. Li, G.P. Peterson, P. Cheng, Dynamic characteristics of transient boiling on a square platinum microheater under millisecond pulsed heating, Int. J. Heat Mass Transf. 51 (2008) 273–282.
[3] Y.B. Tao, Y.L. He, Y.K. Liu, W.Q. Tao, Performance optimization of two-stage latent heat storage unit based on entransy theory, Int. J. Heat Mass Transf. 77 (2014) 695–703.
[4] L.H. Yang, X.J. Quan, P. Cheng, Z.M. Cheng, A free energy model and availability analysis for onset of condensation on rigid and liquid surfaces in moist air, Int. J. Heat Mass Transf. 78 (2014) 460–467.
[5] P.S. Jensen, Finite difference techniques for variable grids, Comput. Struct. 2 (1972) 17–29.
[6] T. Liszka, J. Orkisz, The finite difference method at arbitrary irregular grids and its application in applied mechanics, Comput. Struct. 11 (1980) 83–95.
[7] G.R. Liu, J. Zhang, H. Li, K.Y. Lam, B.B.T. Kee, Radial point interpolation based finite difference method for mechanics problems, Int. J. Numer. Methods Eng. 68 (2006) 728–754.
[8] M. Cui, W.W. Duan, X.W. Gao, A new inverse analysis method based on a relaxation factor optimization technique for solving transient nonlinear inverse heat conduction problems, Int. J. Heat Mass Transf. 90 (2015) 491–498.
[9] M. Cui, K. Yang, X.L. Xu, S.D. Wang, X.W. Gao, A modified Levenberg-Marquardt algorithm for simultaneous estimation of multi-parameters of boundary heat flux by solving transient nonlinear inverse heat conduction problems, Int. J. Heat Mass Transf. 97 (2016) 908–916.
[10] O.C. Zienkiewicz, R.L. Taylor, The Finite Element Method, McGraw-Hill, London, 1989.
[11] T.J.R. Hughes, The Finite Element Method: Linear Static and Dynamic Finite Element Analysis, Prentice-Hall, New Jersey, 1987.
[12] T. Belytschko, W.K. Liu, B. Moran, K. Elkhodary, Nonlinear Finite Elements for Continua and Structures, John Wiley & Sons, New York, 2000.
[13] G.R. Liu, S.S. Quek, The Finite Element Method: A Practical Course, Second ed., Butterworth-Heinemann, Oxford, 2013.
[14] P.B. Bochev, M.D. Gunzburger, Least-Squares Finite Element Methods, Springer, New York, 2009.
[15] J. Lv, G.Y. Sheng, X.W. Gao, H.W. Zhang, Numerical integration approach based on radial integration method for general 3D polyhedral finite elements, Int. J. Comput. Methods 12 (2015) 1550026.
[16] C.A. Brebbia, J.C. Telles, L.C. Wrobel, Boundary Element Techniques, Springer, Berlin, 1984.
[17] P.K. Banerjee, Boundary element method, McGraw-Hill, New York, 1992.
[18] E. Divo, A.J. Kassab, Boundary Element Method for Heat Conduction: With Applications in Non-Homogenous Media, WIT Press, Southampton, 2003.
[19] V. Sladeka, J. Sladeka, M. Tanakab, C. Zhang, Transient heat conduction in anisotropic and functionally graded media by local integral equations, Eng. Anal. Bound. Elem. 29 (2005) 1047–1065.
[20] X.W. Gao, H.F. Peng, J. Liu, A boundary-domain integral equation method for solving convective heat transfer problems, Int. J. Heat Mass Transf. 63 (2013) 183–190.
[21] X.W. Gao, W.Z. Feng, B.J. Zheng, K. Yang, An interface integral equation method for solving general multi-medium mechanics problems, Int. J. Numer. Methods Eng. 107 (2016) 696–720.
[22] X.W. Gao, An effective method for numerical evaluation of general 2D and 3D high-order singular boundary integrals, Comput. Meth. Appl. Mech. Eng. 199 (2010) 2856–2864.

[23] Y.T. Gu, G.R. Liu, A meshfree weak-strong (MWS) form method for time dependent problems, Comput. Mech. 35 (2005) 134–145.
[24] X. Zhang, X.H. Liu, K.Z. Song, M.W. Lu, Least-square collocation meshless method, Int. J. Numer. Methods Eng. 51 (2001) 1089–1100.
[25] G.R. Liu, An overview on meshfree methods: for computational solid mechanics, Int. J. Comput. Methods 13 (2016) 1630001.
[26] P.H. Wen, M.H. Aliabadi, An improved meshless collocation method for elastostatic and elastodynamic problems, Int. J. Numer. Meth. Biomed. 24 (2008) 635–651.
[27] X.W. Gao, A meshless BEM for isotropic heat conduction problems with heat generation and spatially varying conductivity, Int. J. Numer. Methods Eng. 66 (2006) 1411–1431.
[28] B.J. Zheng, X.W. Gao, K. Yang, C. Zhang, A novel meshless local Petrov-Galerkin method for dynamic coupled thermoelasticity analysis under thermal and mechanical shock loading, Eng. Anal. Bound. Elem. 60 (2015) 154–161.
[29] W. Dai, A new accurate finite difference scheme for Neumann (insulated) boundary condition of heat conduction, Int. J. Therm. Sci. 49 (2010) 571–579.
[30] F. Han, W. Dai, New higher-order compact finite difference schemes for 1D heat conduction equations, Appl. Math. Model. 37 (2013) 7940–7952.
[31] A. Yosaf, S.U. Rehman, F. Ahmad, M.Z. Ullah, A.S. Alshomrani, Eighth-order compact finite difference scheme for 1D heat conduction equation, Adv. Numer. Anal. 2016 (2016) 8376061.
[32] B.R. Baliga, S.V. Patankar, A new finite-element formulation for convection-diffusion problems, Numer. Heat Tranf. A-Appl. 3 (1980) 393–409.
[33] B.R. Baliga, S.V. Patankar, A control volume finite-element method for two dimensional fluid flow and heat transfer, Numer. Heat Tranf. A-Appl. 6 (1983) 245–261.
[34] M. Sheikholeslami, M. Gorji-Bandpy, I. Pop, Soheil Soleimani, Numerical study of natural convection between a circular enclosure and a sinusoidal cylinder using control volume based finite element method, Int. J. Therm. Sci. 72 (2013) 147–158.
[35] M. Sheikholeslami, D.D. Ganji, Hydrothermal Analysis in Engineering Using Control Volume Finite Element Method, Academic Press, London, UK, 2015.
[36] M. Sheikholeslami, K. Vajravelu, M.M. Rashidi, Forced convection heat transfer in a semi annulus under the influence of a variable magnetic field, Int. J. Heat Mass Transf. 92 (2016) 339–348.
[37] M. Sheikholeslami, T. Haya, A. Alsaedi, S. Abelman, Numerical analysis of EHD nanofluid force convective heat transfer considering electric field dependent viscosity, Int. J. Heat Mass Transf. 108 (2017) 2558–2565.
[38] P.L. Bishay, J. Sladek, V. Sladek, X.W. Gao, Analysis of elastic media with voids using a mixed-collocation finite-element method, J. Eng. Mech. 04016119 (2016).
[39] P.H. Wen, P. Cao, T. Korakianitis, Finite block method in elasticity, Eng. Anal. Bound. Elem. 46 (2014) 116–125.
[40] M. Li, P.H. Wen, Finite block method for transient heat conduction analysis in functionally graded media, Int. J. Numer. Methods Eng. 99 (2014) 372–390.
[41] M. Li, A. Monjiza, Y.G. Xu, P.H. Wen, Finite block Petrov-Galerkin method in transient heat conduction, Eng. Anal. Bound. Elem. 60 (2015) 106–114.
[42] N. Fantuzzi, F. Tornabene, Strong formulation finite element method for arbitrarily shaped laminated plates –Part I. Theoretical analysis, Adv. Aircraft Spacecraft Sci. 1 (2014) 125–143.
[43] N. Fantuzzi, New insights into the strong formulation finite element method for solving elastostatic and elastodynamic problems, Curved Layer. Struct. 1 (2014) 93–126.
[44] F. Tornabene, N. Fantuzzi, F. Ubertini, E. Viola, Strong formulation finite element method based on differential quadrature: a survey, Appl. Mech. Rev. 1 (2015) 145–175.
[45] X.W. Gao, Element differential method (EDM) for solving heat conduction problems with varying conductivities and sources, in: Proceedings of 1st Asian Conference on Thermal Sciences, Jeju Island, Mach 26–30, 2017.
[46] X.W. Gao, T.G. Davies, Boundary Element Programming in Mechanics, Cambridge University Press, Cambridge, 2002.